metals

MDPI

Article

Optimization of Copper-Embedded Cathode Collector Bars for Reducing Cathode Voltage Drop and Horizontal Current in Aluminum Electrolysis

Jinfeng Han, Chunchun Dong, Yuran Chen *, Yapeng Kong and Xuemin Liang *

School of Materials Science and Engineering, Zhengzhou University, Zhengzhou 450001, China; jfhan@gs.zzu.edu.cn (J.H.)

* Correspondence: cyr_hu@zzu.edu.cn (Y.C.); lxm_zzu@163.com (X.L.)

Abstract

Aluminum electrolysis is an energy-intensive process in which the cathode voltage drop (CVD) and horizontal current in the molten aluminum layer directly affect energy consumption and cell stability. In this study, a three-dimensional electro-thermal model of a 400 kA prebaked aluminum electrolysis cell was established to optimize copper-embedded cathode collector bars. Using a staged parameter-screening and integrated optimization strategy, the effects of copper rod longitudinal position, diameter, and embedded length on CVD, horizontal current density, cathode surface current uniformity, and thermal response were systematically evaluated. Under the present modeling conditions, the configuration with a longitudinal position of 1.0 m, diameter of 0.05 m, and embedded length of 1.0 m provided a favorable balance between electrical performance and copper consumption. This design reduced the equivalent voltage drop by 142.7 mV and decreased the average horizontal current density in the molten aluminum layer to approximately 4900 A/m^2. The peak cathode surface current density was also reduced, corresponding to a predicted cathode service-life increase of approximately 13.2% based on a relative wear model. A preliminary economic analysis indicated that an initial investment of CNY 424,000 could yield conservative annual electricity cost savings of approximately CNY 114,000, with a simple payback period of about 3.7 years. These results provide quantitative guidance for the structural design and industrial evaluation of copper-embedded cathode collector bars.

Keywords: aluminum electrolysis cell; copper-embedded cathode; horizontal current; energy saving; cathode lifespan

Check for updates

Academic Editor: Branimir N. Grgur

Received: 15 May 2026
Revised: 5 June 2026
Accepted: 8 June 2026
Published: 10 June 2026

Copyright: © 2026 by the authors. Licensee MDPI, Basel, Switzerland. This article is an open access article distributed under the terms and conditions of the Creative Commons Attribution (CC BY) license.

1. Introduction

The aluminum electrolysis industry is an essential part of modern industrial production and plays an important role in the global economy [1]. However, conventional primary aluminum production is highly energy-intensive [2]. In the context of climate change mitigation and increasing pressure on energy supply, improving the energy efficiency of aluminum electrolysis has become an urgent priority [3,4]. Stable operation of the electrolysis cell is a prerequisite for achieving superior technical performance and economic viability, and it serves as a critical foundation for reducing energy consumption [5]. Among the factors affecting cell stability, fluctuations of the molten aluminum layer are particularly critical [6,7]. Severe metal pad motion may deform the metal–electrolyte interface, resulting in significant cell voltage oscillations [8]. Consequently, aluminum reduction cells often

have to operate at a larger anode–cathode distance (ACD), which further increases energy consumption. Therefore, suppressing molten aluminum layer fluctuations has become an important research focus for improving the energy efficiency of aluminum electrolysis.

The interaction between horizontal currents and magnetic fields contributes significantly to the motion of molten aluminum within electrolysis cells [9]. To mitigate metal pad motion, three principal strategies have been proposed: increasing hydrodynamic damping, optimizing the magnetic field distribution, and reducing the horizontal current in the molten aluminum layer [10,11]. One approach to enhancing hydrodynamic damping is to modify the cathode geometry, for example by using non-uniform or barrier-type cathode structures, which has been shown to effectively suppress aluminum layer movement and lower the cathode voltage drop [12]. Liu et al. [13] established a three-dimensional two-phase interface model to analyze the flow field and reported that block cathodes reduced the average metal velocity by approximately 60%, while the interface deformation was reduced by around 0.01 m. Curved cathodes have also exhibited stronger damping than flat designs, reportedly lowering DC energy consumption to as low as 12,178 kWh/t-Al. Besides cathode geometry, busbar configuration is another recognized approach to control the vertical magnetic field and restrain aluminum flow fluctuations [14]. Technologies such as the AP60 and APXe cells use shared busbar systems to compensate for magnetic field imbalance, achieving maximum flow velocities of 18.2 cm/s and 22 cm/s, respectively. Although magnetic field optimization and structural damping are theoretically effective, their practical adoption is often constrained by technical complexity and cost. In comparison, reducing the horizontal current in the molten aluminum layer is a more direct and practical route, which has garnered increasing research attention in recent years [15–17].

Structural optimization of the cathode has been identified as an effective route to suppress the horizontal current in the molten aluminum layer [18]. Research efforts have focused on various modifications, including increasing the height of the cathode collector bars [19,20], elevating side carbon blocks [21], and optimizing the materials, geometry, and assembly of cathode components [22]. Among these approaches, introducing highly conductive copper inserts into the cathode collector bar is considered a particularly promising strategy [23,24]. Von Kaenel et al. [25] demonstrated that embedding copper inserts into steel collector bars improved the uniformity of horizontal current distribution. Bastaki et al. [26] reported that a combination of modifications, including copper rod embedding, led to a reduced voltage drop, with copper embedding highlighted as one of the most effective individual measures. Similarly, Gupta [27] showed that modifying steel bars with copper rods yielded a more uniform surface current distribution and extended cathode lifespan. Consequently, the use of copper-embedded steel cathode rods is now considered one of the most practical and effective strategies for mitigating horizontal current and enhancing cathode durability. However, quantitative design guidelines for copper-embedded cathode collector bars remain insufficient. In particular, the effects of key geometric parameters, including copper insert diameter, embedded length, and longitudinal position, on cathode voltage drop, horizontal current suppression, and cathode surface current uniformity have not been fully quantified. Moreover, comprehensive evaluations that balance electrical benefits, copper consumption, and thermal impact remain limited, hindering the engineering optimization and economic application of this technology.

Although copper-embedded collector bars have been reported to improve current redistribution, voltage-drop reduction, and cathode durability, systematic design guidelines for their geometric parameters remain limited. In particular, the coupled effects of copper insert position, diameter, and embedded length on CVD, horizontal current suppression, current-density uniformity, thermal response, and copper consumption have not been fully evaluated under the same modeling framework. Moreover, the thermal penalty caused

by Joule heat redistribution after copper embedding still requires engineering assessment. Therefore, a quantitative optimization framework that jointly considers electrical performance, thermal response, and copper consumption is still needed to guide the structural design of copper-embedded cathode collector bars.

To address this issue, this study conducted a systematic parametric investigation of copper-embedded cathode collector bars. A three-dimensional electro-thermal model of a 400 kA industrial aluminum electrolysis cell was established to quantitatively evaluate the effects of copper rod diameter, length, and positioning on the cathode voltage drop, horizontal current density in the molten aluminum layer, and cathode surface current uniformity. Based on these results, a recommended configuration was identified under the present modeling conditions by considering voltage-drop reduction, horizontal current suppression, current distribution uniformity, copper usage, and thermal response. Furthermore, we extend the analysis to evaluate the corresponding impact on cathode service life and cell thermal balance, culminating in a comprehensive techno-economic assessment. These results provide a numerical basis for the design and further industrial validation of copper-embedded cathodes, supporting their potential application in energy-efficient and low-carbon aluminum electrolysis.

2. Methods

2.1. Aluminum Electrolysis Cell Model and Mesh Generation

A three-dimensional finite element slice model was developed based on a 400 kA prebaked anode aluminum electrolysis cell operated in an industrial plant in Henan Province, China. All geometric modeling and numerical calculations were performed using ANSYS 2021 R1 finite-element software. Considering the high computational cost of modeling the full-scale cell and the focus of this study on the effects of copper embedding on the local current-collection path, cathode voltage drop, and horizontal current component in the molten aluminum layer, a representative slice containing typical anode, cathode, molten aluminum, and electrolyte regions was selected as the computational domain.

The model included the main components of the cell, namely the anode assembly, consisting of the carbon block, guide rod, and steel claw; the cathode assembly, consisting of the cathode carbon block and steel collector bar; the molten aluminum layer; the electrolyte; the insulation layer; and the side ramming paste. This model was mainly used to compare the relative effects of different copper-embedded cathode configurations under identical boundary conditions. The main geometric parameters are listed in Table 1.

Table 1. Key structural parameters of the 400 kA aluminum electrolysis cell model.

Component	Parameter	Value (m)
Anode	Carbon block (L × W × H)	1.6 × 0.7 × 0.56
	Guide rod (L × W × H)	1.2 × 0.14 × 0.14
	Steel claw (L × W × H)	1.16 × 0.14 × 0.46
Cathode	Cathode carbon block (L × W × H)	3.55 × 0.7 × 0.45
	Cathode steel collector bar (L × W × H)	2.1 × 0.09 × 0.18
Others	Cover material thickness	0.15

The computational domain was discretized using tetrahedral elements. Local mesh refinement was applied to the steel collector bar, copper insert, cathode carbon block, and molten aluminum region, as these regions directly affect the cathode current-collection path, cathode voltage drop, and horizontal current distribution in the molten aluminum layer. In particular, the copper–steel interface and the connection region between the steel

collector bar and the cathode carbon block were refined because relatively large potential gradients may occur in these areas.

The electrical boundary conditions were defined according to the cathode slice model. Since the full cell current was 400 kA and the cell contained 48 cathode blocks, a current of approximately 8333 A was applied to the anode aluminum stem in the single-slice model. The outlet end of the cathode steel collector bar was set as the reference potential, with an electric potential of 0 V. The same electrical boundary conditions were used for all simulation cases to ensure the comparability of different copper-insert configurations.

A mesh-independence study was conducted by progressively refining the global mesh. The cathode voltage drop and the average horizontal current density in the molten aluminum layer were selected as the evaluation criteria. After the mesh was refined from the medium mesh to the fine mesh, the variations in cathode voltage drop and average horizontal current density were 0.15% and 1.14%, respectively. Both values were less than 3%, indicating that the numerical results were no longer sensitive to further mesh refinement. Therefore, the medium mesh, consisting of 172,583 nodes and 55,314 elements, was selected for the subsequent simulations, with local refinement mainly applied to the cathode assembly region, as shown in Figure 1. The detailed mesh-independence data are provided in Table S1 in the Supporting Information.

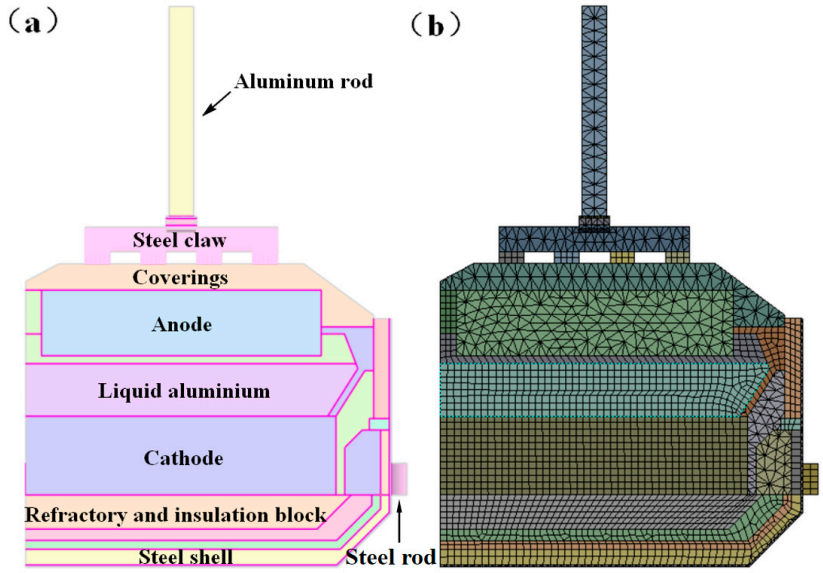

Figure 1. Schematic of the electrolysis cell: (**a**) geometric structure and (**b**) computational mesh.

2.2. Optimization Strategy for the Copper-Embedded Cathode Structure

The uniformity of current distribution in the cathode assembly is closely related to the geometric parameters of the copper insert, including its location and size. To systematically optimize the copper-embedded cathode design, a parameter study combining position screening and size optimization was adopted. Three key variables were selected: (1) the longitudinal position of the copper rod, D_L; (2) the copper rod length, L; and (3) the copper rod diameter, D. These parameters are defined schematically in Figure 2. In the model, the copper–steel interface was treated as a directly mechanically contacted interface with good electrical contact. Therefore, an effective electrical connection between the copper rod and the steel collector bar was assumed, allowing the copper rod to participate in cathode current collection as a low-resistance pathway. The simulation procedure consisted of two stages.

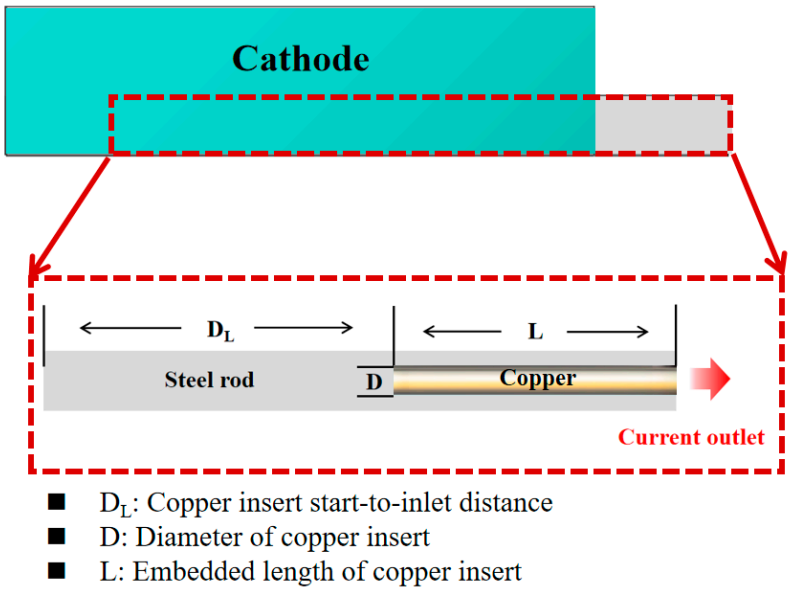

Figure 2. Schematic diagram defining the longitudinal position D_L, embedded length L, and diameter D of the copper rod.

2.2.1. Stage 1: Analysis of the Effect of Copper Rod Position

In the first stage, the copper rod length and diameter were fixed at L = 0.4 m and D = 0.05 m, respectively. The longitudinal position D_L was varied from 0 m, corresponding to the innermost end of the steel collector bar near the cell center, toward the outer side of the steel bar, away from the cell center, in increments of 0.1 m until the current outlet end of the steel collector bar was reached. For each position, the cathode voltage drop and the average horizontal current density in the molten aluminum layer were calculated. By comprehensively evaluating these two key indicators, the preferred longitudinal position range of the copper rod was identified and used as the basis for the subsequent size optimization.

2.2.2. Stage 2: Parametric Analysis of Copper Rod Length and Diameter

Based on the preferred position range determined in the first stage, a parametric combination method was used to systematically investigate the coupled effects of copper rod length L and diameter D. The copper rod lengths were set as 0.4, 0.7, 1.0, 1.3, and 1.8 m, while the diameters were set as 0.02, 0.03, 0.05, 0.06, and 0.07 m. Each (L,D) combination was placed within the preferred position region for calculation. The cathode voltage drop, average horizontal current density in the molten aluminum layer, and cathode surface current distribution uniformity were then obtained. Through comparative analysis, quantitative relationships between the geometric parameters of the copper rod and the key performance indicators of the electrolysis cell were established. The key varied parameters and fixed modeling conditions used in the numerical parametric study are summarized in Table S2 in the Supporting Information.

All copper-embedded configurations were calculated using the same ANSYS-based finite-element settings. The total length of the cathode steel collector bar was 2.1 m, and the definitions of D_L, L, and D are shown in Figure 2.

To make the numerical investigation procedure clearer, the overall methodology framework of this study is shown in Figure 3. The workflow includes baseline cell modeling, boundary-condition definition, mesh-independence verification, copper rod position screening, copper rod length and diameter optimization, electrical-performance evaluation,

thermal impact analysis, cathode service-life estimation, economic feasibility assessment, and recommended configuration determination.

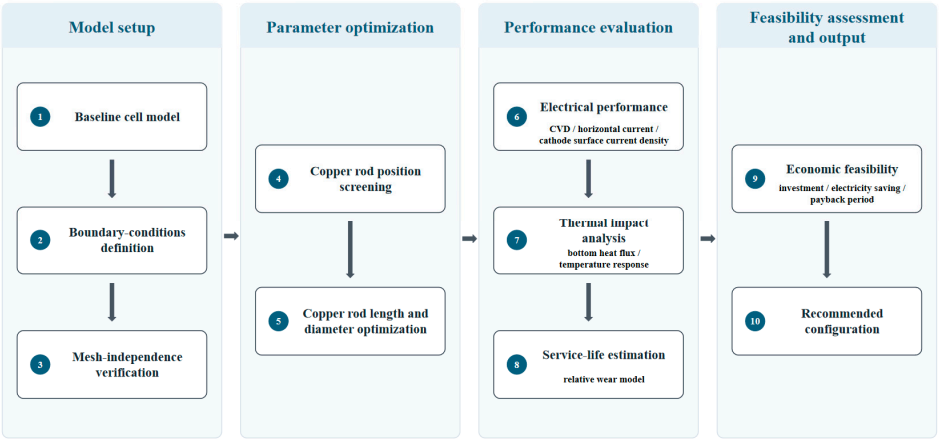

Figure 3. Methodology framework for the numerical optimization of copper-embedded cathode collector bars.

2.3. Governing Equations and Numerical Methods

2.3.1. Thermal Field Analysis

The temperature field of the aluminum electrolysis cell was solved using the three-dimensional steady-state heat conduction equation. Internal Joule heat generation in the solid components and heat losses from the external boundaries were considered in the model. Because strong natural convection exists in the electrolyte and molten aluminum regions, these domains were approximately treated as isothermal domains in the thermal calculation. The governing equation for heat conduction can be expressed as follows [28,29]:

$$\lambda_x \frac{\partial^2 T}{\partial x^2} + \lambda_y \frac{\partial^2 T}{\partial y^2} + \lambda_z \frac{\partial^2 T}{\partial z^2} + q_{vol} = 0 \quad (1)$$

where λ_x, λ_y, λ_z are the thermal conductivities of the material in the x, y, z directions, respectively. T is temperature, and q_{vol} is the volumetric Joule heat generation rate.

All external surfaces of the cell model were assigned third-type, or Robin, boundary conditions for convective heat transfer:

$$-\lambda_n \frac{\partial T}{\partial n} = \alpha(T - T_E) \quad (2)$$

where λ_n is the thermal conductivity normal to the surface, α is the convective heat transfer coefficient, T_E is the ambient temperature, and n denotes the outward normal direction.

The convective heat transfer coefficients for surfaces exposed to ambient air or flowing flue gases were determined based on empirical correlations involving the Nusselt number (Nu). The characteristic length (L_c) for these correlations was defined as:

$$L_c = \frac{A_P}{P} \quad (3)$$

where A_P is the heat transfer surface area and P is its perimeter. The heat transfer coefficient was then calculated as:

$$\alpha = \frac{\lambda_{fluid} \cdot Nu}{L_c} \quad (4)$$

where λ_{fluid} is the thermal conductivity of the fluid.

2.3.2. Electric Field Analysis

The electric potential distribution was calculated under steady-state conditions by solving the Laplace equation derived from charge conservation in all conductive domains [18,30]:

$$\sigma_x \frac{\partial^2 V}{\partial x^2} + \sigma_y \frac{\partial^2 V}{\partial y^2} + \sigma_z \frac{\partial^2 V}{\partial z^2} = 0 \quad (5)$$

where V is the electric potential, and σ_x, σ_y and σ_z are the electrical conductivities in the principal directions.

The electrical boundary conditions were defined as follows. The first-type boundary condition was used to prescribe a fixed electric potential:

$$V(x, y, z) = V_b(x, y, z) \quad (6)$$

The second-type boundary condition was used to prescribe the normal current density at the boundary:

$$-\sigma_n \frac{\partial V}{\partial n} = -J(x, y, z) \quad (7)$$

where J is the current density normal to the surface, and σ_n is the conductivity in the normal direction.

The computational domain was discretized into finite elements. The Galerkin weighted residual method was applied to discretize the governing equation and boundary conditions, yielding the global finite element equation:

$$[K]\{V\} = \{F\} \quad (8)$$

where $[K]$ is the global conductance matrix, $\{V\}$ is the vector of nodal potentials, and $\{F\}$ is the load vector accounting for the boundary conditions. This system was solved using a direct solver in the ANSYS environment to obtain the potential distribution, from which the current density and Joule heat source (q_{vol} in Equation (1)) were derived.

3. Results and Discussion

3.1. Effect of Copper Embedding on Cathode Voltage Drop

To quantify the influence of the copper insert on the cathode voltage drop (CVD), the three-dimensional electric potential distribution in the baseline cathode structure without copper embedding was first simulated. As shown in Figure 4, the current flowed from the surface of the cathode carbon block, converged through the carbon block into the steel collector bar, and was then extracted through the collector bar. Along the current path, the electric potential gradually decreased from approximately 203.7 mV to nearly zero, resulting in a baseline CVD of 203.7 mV. The potential distribution indicates that the potential variation was relatively concentrated near the contact region between the steel collector bar and the carbon block during current collection. This region is therefore an important contributor to the ohmic voltage drop and a key area for current collection into the steel collector bar.

The CVD can be effectively regulated by optimizing the longitudinal position D_L of the embedded copper rod. As shown in Figure 5, when a copper rod with a fixed length of 0.4 m was shifted from the cell-center side (D_L = 0 m) toward the outer side of the steel collector bar in increments of 0.1 m, the CVD exhibited a distinct non-monotonic trend. Increasing D_L from 0 to 1.0 m led to a gradual reduction in CVD from approximately 203 mV to 195 mV, indicating improved current collection efficiency. A more pronounced decrease was observed as D_L further increased to 1.5 m, where the CVD dropped to approximately 165 mV. This marked reduction is related to the highly conductive copper

rod being positioned closer to the main current-collection region, thereby shortening the current path through the higher-resistance steel collector bar. However, when D_L exceeded 1.6 m, the CVD began to increase. This is because the copper rod extended beyond the primary current-collection region of the cathode carbon block, diminishing its effectiveness in capturing the vertical current. Therefore, positioning the copper rod within D_L = 1.0–1.3 m is more favorable for subsequent size optimization because it provides a reasonable compromise between enhancing conduction efficiency and maintaining overall cell performance.

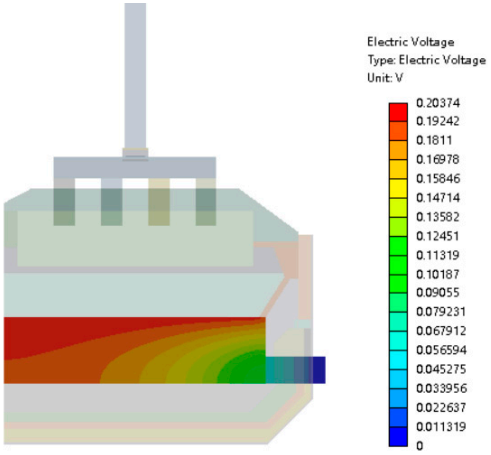

Figure 4. Schematic of the electric potential distribution in the cathode region of the aluminum electrolysis cell.

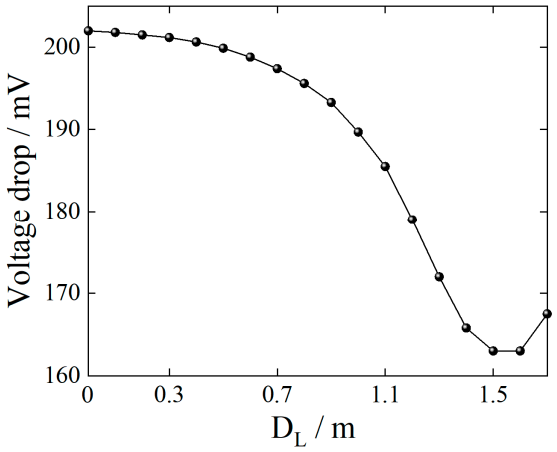

Figure 5. Cathode voltage drop as a function of the longitudinal position D_L of the copper rod for a fixed rod length of 0.4 m.

Based on the determined favorable positional range, the coupled effects of copper rod length L and diameter D on the reduction in CVD were systematically investigated, as shown in Figure 6. For a fixed rod length L, increasing the copper rod diameter D led to a pronounced and nearly monotonic reduction in CVD. As D increased from 0.02 m to 0.07 m, the CVD reduction increased from nearly zero to approximately 50–110 mV, indicating that enlarging the cross-sectional area of the copper insert is an effective approach for reducing the CVD.

At a fixed diameter D, increasing the copper rod length L also enhanced the voltage-drop reduction. When D $\geq$ 0.02 m, the differences among the curves corresponding to different rod lengths became more pronounced. At D = 0.07 m, the voltage-drop reduction for the L = 1.8 m configuration was more than twice that for the L = 0.4 m configuration, suggesting a coupled effect between increasing the diameter and extending the embedded

length. However, when L was increased from 1.3 m to 1.8 m, the additional reduction in CVD became less evident, indicating a diminishing marginal benefit.

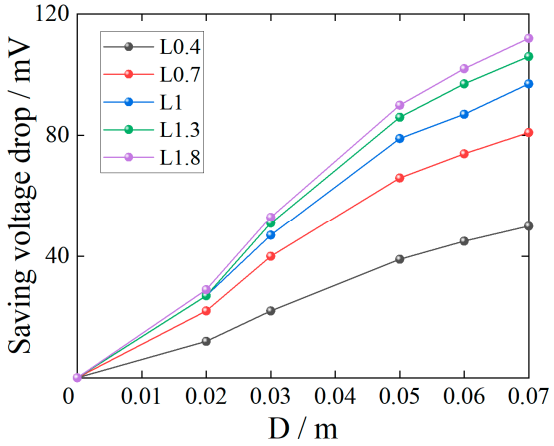

Figure 6. Reduction in cathode voltage drop as a function of copper rod diameter for various embedded lengths.

This behavior can be interpreted from the perspective of current-path redistribution. Increasing the diameter and length of the highly conductive copper insert enables it to carry a larger proportion of the vertical current, thereby diverting part of the current that would otherwise flow through the higher-resistance steel collector bar and carbon block. As a result, the local ohmic voltage drop is reduced. Once the copper insert sufficiently covers the main current-collection region of the cathode, further increasing its length has a limited effect on improving the overall current distribution. Therefore, the diameter D and length L of the copper rod are key geometric parameters affecting the CVD. Based on the above results, a relatively large diameter ($D \geq 0.05$ m) combined with a moderate length (L = 1.0–1.3 m) is recommended to obtain a favorable reduction in CVD while maintaining reasonable copper consumption, thereby contributing to the energy-efficient design of copper-embedded cathodes.

3.2. Suppression of Horizontal Current in Molten Aluminum

In addition to reducing the cathode voltage drop, another important function of the highly conductive copper rod is to suppress the horizontal current density in the molten aluminum layer. The interaction between the horizontal current in the molten aluminum and the magnetic field generates Lorentz forces, which are an important factor inducing molten aluminum motion. Therefore, this section evaluates the effectiveness of the copper insert in suppressing the horizontal current. Figure 7 illustrates the current flow path within the electrolysis cell. The current enters the molten aluminum layer approximately vertically at the aluminum–electrolyte interface, then deflects toward the cathode carbon block, forming a horizontal current component in the molten aluminum layer, and is finally collected and extracted through the cathode steel collector bar.

The average horizontal current density in the molten aluminum layer was strongly affected by the longitudinal position D_L of the copper rod. Figure 8 shows the variation in average horizontal current density with D_L when the copper rod dimensions were fixed at L = 0.4 m and D = 0.05 m. A distinct minimum was observed. When D_L increased from 0 to 1.0 m, the average horizontal current density decreased from 9292 A/m^2 to 8588 A/m^2. This suppression effect is attributed to the improved current-collection efficiency provided by the properly positioned highly conductive copper rod, which offers a preferential low-resistance pathway for vertical current and thereby reduces the need for lateral current flow in the molten aluminum layer. However, when the copper rod moved further outward

beyond the position corresponding to the lower average horizontal current density in this model ($D_L \approx 1.0$ m), the suppression effect gradually weakened. When D_L increased to 1.7 m, the average horizontal current density increased to 9650 A/m^2, approximately 12.4% higher than the minimum value. This increase occurs because, when the copper rod is placed too far from the main current-collection region, its ability to shunt the vertical current decreases, causing a larger proportion of the current to flow horizontally in the molten aluminum layer before reaching a low-resistance current-collection path.

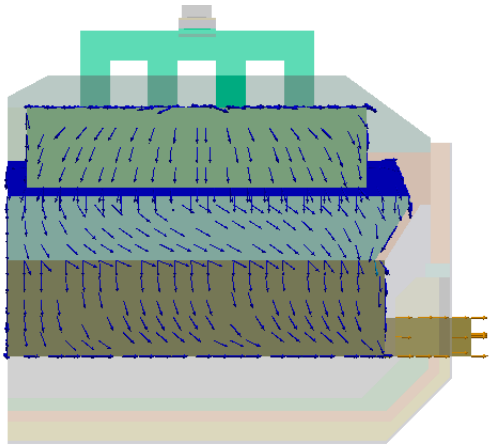

Figure 7. Schematic of the current flow path within the aluminum electrolysis cell.

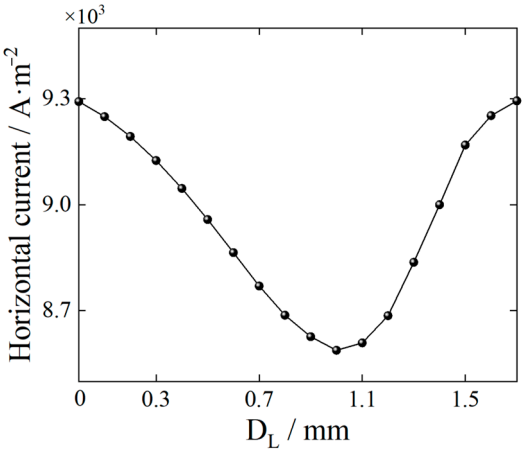

Figure 8. Average horizontal current density in the molten aluminum layer as a function of the longitudinal position D_L of the copper rod.

To clarify the influence of copper rod geometry on horizontal current suppression, a parametric study was conducted at D_L = 1.0 m, as shown in Figure 9. For any fixed rod length L, increasing the copper rod diameter D significantly and monotonically reduced the average horizontal current density in the molten aluminum layer. Taking D_L = 1.0 m and L = 1.0 m as an example, when D increased from 0.02 m to 0.07 m, the current density decreased by approximately 25%. In addition, at a fixed diameter D, increasing the copper rod length L also effectively reduced the average horizontal current density. When D > 0.02 m, the differences among the curves corresponding to different rod lengths became pronounced. For example, at D = 0.07 m, the current density for the L = 1.8 m configuration was approximately 2.0 × 10^3 A/m^2, about 65% lower than that for the L = 0.4 m configuration. This coupled effect indicates that sufficient cross-sectional area and appropriate embedded length are both essential for effective current shunting in the molten aluminum layer. It should also be noted that when L exceeded 1.3 m, the additional improvement caused by further increasing the rod length became much smaller, indicating that the

current-shunting effect tended to stabilize once the copper insert sufficiently covered the core current-collection region.

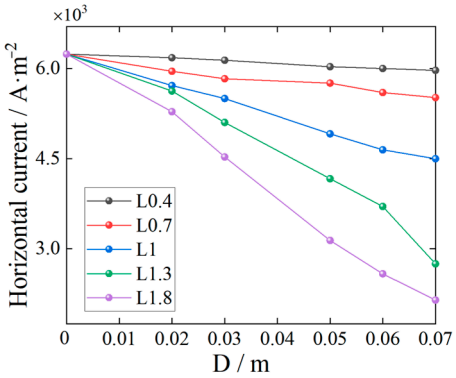

Figure 9. Average horizontal current density in the molten aluminum layer as a function of copper rod diameter for various embedded lengths.

The above results indicate that the mechanism by which the copper insert suppresses the horizontal current is the formation of a local low-resistance current-shunting pathway. By constructing an efficient vertical conduction path in the main current-collection region, the copper insert reduces the current component that must flow laterally through the molten aluminum layer. Therefore, the optimization direction of copper rod position and geometry for horizontal current suppression is highly consistent with that for reducing the cathode voltage drop. Considering both performance improvement and material economy, placing the copper rod within D_L = 1.0–1.3 m can effectively suppress the horizontal current in the molten aluminum layer while also contributing to the energy-saving design of the cathode structure.

3.3. Current Density Uniformity and Cathode Service-Life Extension

The current density distribution on the surface of the cathode carbon block is an important factor affecting cathode service life, because localized high current density can accelerate carbon block wear and erosion. This section analyzes the effect of copper embedding on the cathode surface current density distribution and further evaluates its potential influence on cathode service life.

The non-uniform characteristics of the cathode surface current density are shown in Figure 10. The current density profile was extracted along a vertical probe line on the cathode surface toward the steel collector bar outlet. A pronounced current density peak was observed near the side ledge region. This peak is mainly related to current convergence toward the low-resistance collector-bar region and local current deflection caused by the electrically non-conductive side ledge. Similar effects of cathode geometry and collector-bar configuration on current redistribution have been reported in previous numerical studies [12,15]. In addition, the side ledge, owing to its much lower electrical conductivity than the carbon cathode and molten aluminum, can constrain the local current path and modify the current-density distribution [27,31]. Therefore, the peak in Figure 10 can be attributed to the coupling between the low-resistance current-collection path and the side-ledge-induced current redistribution.

After embedding the copper rod, the current density distribution on the cathode surface changed noticeably. Figure 11 shows the variation in the maximum cathode surface current density (J_{max}) with copper rod diameter D and length L. For any fixed length L, increasing the copper rod diameter D significantly reduced J_{max}. Taking L = 1.0 m as an example, when D increased from 0.02 m to 0.07 m, J_{max} decreased from 27,343 A/m^2 to 19,543 A/m^2, corresponding to a reduction of 28.5%. At a fixed diameter D, increasing the

copper rod length L also contributed to a reduction in J_{max}. When L increased from 0.4 m to 1.0 m, the average reduction in J_{max} across different diameters was 23.7%. However, when L exceeded 1.3 m, the improvement in current density uniformity became less pronounced. This indicates that once the copper insert basically covered the main current-collection region, further increasing its length produced only limited additional improvement in cathode surface current uniformity.

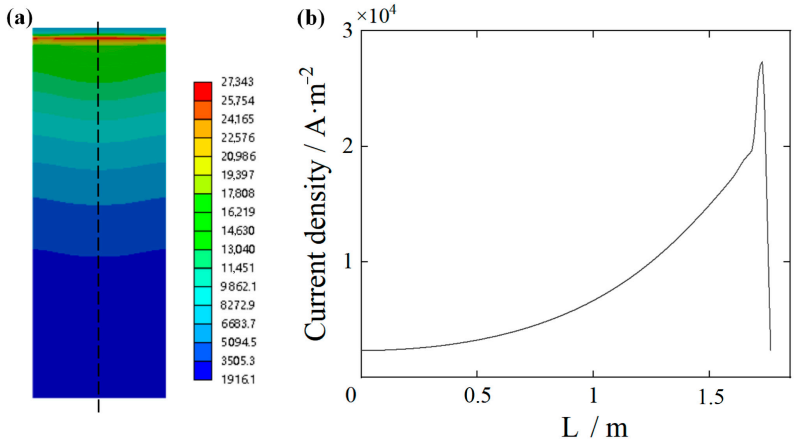

Figure 10. (**a**) Location of the vertical probe line on the cathode surface and (**b**) the corresponding current density profile through the cathode carbon block.

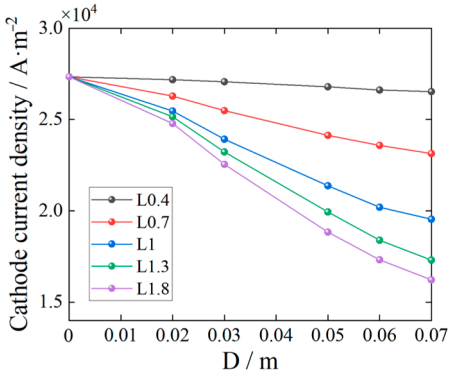

Figure 11. Maximum cathode surface current density Jmax as a function of copper rod diameter for various embedded lengths.

The reduction in peak current density is generally beneficial for weakening localized current crowding in the cathode carbon block, thereby reducing the risk of local wear. The wear rate of cathode carbon blocks is commonly positively correlated with local current density. Based on an empirical model established from industrial operating data [12], the wear rate W can be expressed as a function of current density J:

$$W = 0.015ln(J) - 0.108 \quad (9)$$

Using a baseline cathode service life of 6 years for the configuration without copper embedding, the current-density-related wear model was used to estimate the trend in cathode service life for different copper-embedded configurations. The results are shown in Figure 12. The predicted cathode service life increased continuously as the copper insert size, including diameter D and length L, increased. For the largest configuration (D = 0.07 m, L = 1.8 m), the predicted service life reached 7.26 years, more than 1.2 years longer than the baseline value. Considering both energy-saving potential and material

economy, the recommended configuration (D = 0.05 m, L = 1.0 m) gave a predicted service life of approximately 6.8 years, corresponding to a service-life increase of about 13.2%.

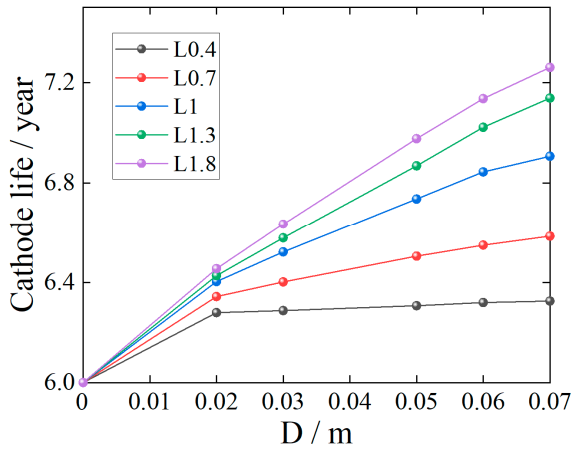

Figure 12. Predicted cathode service life for different copper rod diameters and lengths.

In conclusion, embedding copper in the cathode steel collector bar helped homogenize the cathode surface current density distribution and alleviate local current crowding. This change suggests a potential reduction in the local electrochemical wear rate of the cathode carbon block, which may contribute to extending cathode service life and reducing relining-related costs. It should be noted that the service-life estimation is based on an empirical wear model and is mainly used for relative comparison among different copper-embedded configurations. The actual service-life improvement still needs to be verified using long-term industrial operating data.

3.4. Thermal Impact and Insulation Strategy

The introduction of highly conductive copper into the cathode assembly changes the current path and the spatial distribution of Joule heat, thereby affecting the thermal balance of the electrolysis cell. To maintain stable cell operation, it is necessary to evaluate the thermal influence associated with this improvement in electrical performance and to develop appropriate insulation adjustment strategies.

Figure 13 shows the simulated temperature distribution of the baseline cell without copper embedding. A clear temperature gradient was observed inside the cell. The region near the connection between the cathode steel collector bar and the carbon block exhibited a relatively pronounced local thermal effect, which is related to current collection and interfacial resistance at the steel collector bar–carbon block connection. Because the local peak temperature is sensitive to contact resistance, Joule heat allocation, and thermal boundary conditions, the present study focuses mainly on the relative change in bottom heat flux caused by copper embedding rather than on the absolute maximum temperature.

The introduction of the copper insert significantly changed the bottom heat flux of the cell. As shown in Figure 14, for any fixed embedded length L, increasing the copper rod diameter D led to a marked increase in the cathode bottom heat flux. This behavior can be explained by the low-resistance pathway provided by the highly conductive copper rod. Part of the current that originally flowed through the higher-resistance steel collector bar and carbon block was diverted through the copper insert, reducing local Joule heat generation inside the cathode assembly. Consequently, a larger fraction of the input energy was dissipated through the cell bottom in the form of heat flux.

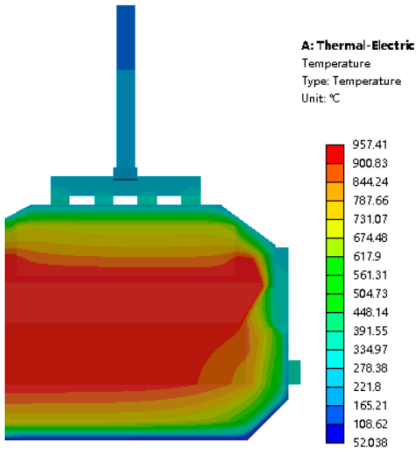

Figure 13. Simulation of temperature distribution in the aluminum electrolysis cell.

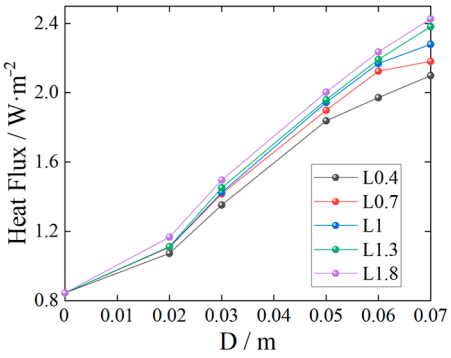

Figure 14. Cathode heat flux as a function of copper rod diameter for various embedded lengths.

For example, under the largest investigated configuration (L = 1.3 m, D = 0.07 m), the simulated bottom heat flux reached 23,819 W/m^2, which was approximately 182% higher than the baseline value of 8438.7 W/m^2. Such a substantial increase in bottom heat loss may lower the overall internal temperature of the cell if no compensation measures are adopted. This may further lead to excessive side ledge growth, increased electrolyte resistance, and reduced operational stability. Therefore, aluminum electrolysis cells using copper-embedded cathodes should be accompanied by enhanced insulation measures. In engineering practice, the thermal balance can be compensated by adjusting the cover material thickness and optimizing the bottom and side insulation structures. In cases where the increase in heat loss is large, it may also be necessary to improve the bottom insulation structure, for example, by increasing the thickness of insulation materials or selecting materials with lower thermal conductivity, thereby increasing the overall thermal resistance and compensating for the increased bottom heat loss.

4. Comprehensive Analysis and Recommended Design

Based on the results regarding cathode voltage drop, horizontal current suppression in the molten aluminum layer, cathode service life, and thermal balance, this study proposes a recommended range of design parameters under the present modeling conditions. A preliminary economic feasibility assessment was further conducted for the recommended configuration, with the aim of providing a design basis that combines technical advancement and engineering practicality for the industrial application of copper-embedded cathode technology.

4.1. Determination of the Recommended Design Range

The simulation results indicate that embedding a copper rod into the cathode steel collector bar can, to a certain extent, synergistically improve three key indicators: (1) reducing the cathode voltage drop; (2) suppressing the horizontal current density in the molten aluminum layer; and (3) homogenizing the cathode surface current density distribution, which is beneficial for extending cathode service life. These improvements are mainly controlled by three geometric parameters of the copper rod: the longitudinal position D_L, diameter D, and length L.

- Recommended embedding position (D_L)

The longitudinal position is a key factor regulating current-collection efficiency. Placing the copper rod within D_L = 1.0–1.3 m provides a favorable balance between reducing the cathode voltage drop, with an average reduction greater than 30 mV, and decreasing the average horizontal current density in the molten aluminum layer, with a reduction greater than 600 A/m^2. In this position range, the copper rod can effectively intercept part of the vertical current, shorten its path through the higher-resistance steel collector bar, and reduce the horizontal current component in the molten aluminum layer.

- Recommended geometric dimensions (D,L)

Within the recommended D_L range, increasing the copper rod diameter D and length L generally improves the key performance indicators, but the marginal benefit gradually decreases as the insert size increases. Configurations with L = 1.0–1.3 m and D $\geq$ 0.05 m can obtain most of the performance improvement, including a cathode voltage-drop reduction greater than 140 mV, a decrease in horizontal current density greater than 1000 A/m^2, and a predicted service-life increase greater than 13%. Further increasing L beyond 1.3 m or increasing D may provide additional improvement, but it also increases copper consumption, steel collector bar drilling or grooving difficulty, copper rod assembly difficulty, end-sealing requirements, and the difficulty of controlling copper–steel interfacial contact quality.

- Key considerations for engineering application

The copper–steel interfacial contact resistance is an important factor affecting the actual energy-saving performance. In practical applications, manufacturing quality, interfacial oxidation, thermal cycling, and long-term service conditions may reduce the realized energy-saving effect compared with the idealized simulation results. Therefore, a low-resistance and highly reliable copper–steel interface should be ensured during manufacturing.

Considering the combined effects of performance improvement, material economy, and engineering feasibility, the configuration with D = 0.05 m, L = 1.0 m, and D_L = 1.0 m is recommended under the present modeling conditions. This configuration provides a favorable overall performance while maintaining good manufacturability.

4.2. Economic Analysis of Copper Usage and Energy-Saving Effect

To quantify the relationship between copper input and energy-saving benefit, the copper insert volume fraction, defined as the ratio of copper rod volume to steel collector bar volume, was correlated with the equivalent voltage-drop reduction, as shown in Figure 15. In this plot, configurations located closer to the upper-left region represent a higher voltage-drop reduction at lower copper consumption, indicating better material utilization efficiency.

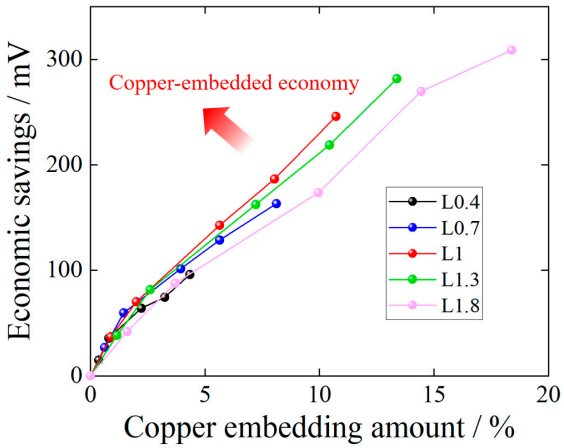

Figure 15. Optimized economy curve of copper embedded fraction versus cell voltage reduction.

The results show that, at the same copper insert volume fraction, increasing the copper rod length L to 1.0 m can markedly improve the energy-saving benefit per unit copper usage. For example, when the copper insert volume fraction was in the range of 5–8%, the L = 1.0 m configuration exhibited better material economy than the L = 0.4 m configuration. Within this range, the voltage-drop reduction for the L = 1.0 m configuration reached 142.7–186.6 mV.

In particular, at a copper insert volume fraction of approximately 5.6%, corresponding to D = 0.05 m and L = 1.0 m, the voltage-drop reduction reached 142.7 mV. This value was 122.8% higher than that of the L = 0.4 m configuration (64.1 mV), while the copper usage was only about half that of the larger L = 1.8 m configuration. In addition, when L = 1.0 m and the copper insert volume fraction was 5–8%, the voltage-drop reduction increased with increasing copper fraction, whereas the decrease in material utilization efficiency was relatively mild, approximately 8.3%. This indicates that this range provides a favorable balance between material input and energy-saving benefit.

Therefore, a copper rod length of L = 1.0 m combined with a copper insert volume fraction of approximately 5–8% provides a suitable balance between copper consumption and voltage-drop reduction. Among these configurations, the design with D = 0.05 m and L = 1.0 m was selected as the recommended configuration for the subsequent economic assessment.

4.3. Preliminary Economic Feasibility Assessment of the Recommended Design

The preliminary economic feasibility of the recommended copper-embedded cathode configuration (D_L = 1.0 m, D = 0.05 m, L = 1.0 m) was evaluated for a 400 kA aluminum electrolysis cell. The key assumptions and calculated results are summarized in Table 2.

The economic feasibility assessment indicates that the recommended copper-embedded cathode configuration (D_L = 1.0 m, D = 0.05 m, L = 1.0 m) has potential for industrial application. Under a conservative scenario, in which only 50% of the theoretical energy-saving effect corresponding to the simulated voltage-drop reduction of 142.7 mV was considered to account for model uncertainty and possible copper–steel interfacial contact losses, the simple payback period was estimated to be within 3.7 years. If additional benefits, such as reduced relining cost associated with extended cathode service life and the residual value of recycled copper after cathode relining, are further considered, the payback period may be shortened to approximately 2.2 years, assuming a copper recovery rate of 90%.

Table 2. Preliminary economic analysis of the recommended copper-embedded cathode design for a 400 kA cell.

Item	Value	Remarks/Basis
Investment Cost		
Cost per copper rod, including material and processing	¥3788	Material: ¥1788; Processing: ¥2000.
Number of cathode steel collector bars per cell	112	
Total Initial Investment	¥424,256	
Annual Operating Benefit		
Simulated equivalent voltage-drop reduction	142.7 mV	From the model for the optimal configuration.
Aluminum production per cell	1105.39 t/year	
Theoretical annual energy saving	504,765.3 kW·h	
Conservative annual energy saving (50% of theoretical)	252,382.65 kW·h	Accounts for model uncertainties and interfacial contact losses.
Electricity price	¥0.45/kW·h	
Conservative annual revenue increase	¥113,572.2	
Payback Period		
Simple payback period	approximately 3.74 years	Initial Investment/Annual Benefit.
Payback period with copper recycling (90% recovery post-relining)	approximately 2.15 years	Considers salvage value of copper.

5. Conclusions

This work provides a quantitative parameter-selection framework for copper-embedded cathode collector bars by jointly considering electrical performance, thermal response, copper consumption, service-life estimation, and economic feasibility. The main conclusions are as follows:

- The optimal design parameters of the copper-embedded cathode were determined as D_L = 1.0 m, D = 0.05 m, and L = 1.0 m. Theoretically, this configuration can achieve a cell voltage reduction of 142.7 mV, while reducing the average horizontal current density in the molten aluminum layer to approximately 4900 A/m^2.
- The copper-embedded design can improve the uniformity of the current density distribution on the cathode surface. Under the optimal copper-embedded configuration, the peak current density was reduced by approximately 10,000 A/m^2, and the predicted cathode service life increased by 13.2%.
- Current shunting by the copper insert reduced Joule heat generation in the cathode, while increasing the bottom heat flux. Under the optimal copper-embedded configuration, the heat flux increased by approximately 48%. Therefore, the cover material thickness should be adjusted and the bottom insulation structure should be optimized to maintain the thermal balance of the cell.
- The initial investment for a single cell was CNY 424,000. Under a conservative scenario, in which 50% of the theoretical energy-saving value was adopted, the annual electricity cost saving was CNY 114,000, and the payback period was approximately 3.7 years. If the reduction in relining cost due to extended cathode service life and the residual value from copper recovery are considered, with a copper recovery rate of 90%, the payback period may be shortened to approximately 2.2 years.

- The present results are based on a steady-state electro-thermal slice model with ideal copper–steel electrical contact, and future work will further consider interfacial contact resistance and industrial operating validation.

Supplementary Materials: The following supporting information can be downloaded at: https://www.mdpi.com/article/10.3390/met16060639/s1, Table S1: Mesh-independence verification for the cathode slice model; Table S2: Key varied parameters and fixed modeling conditions used in the numerical parametric study.

Author Contributions: J.H.: Investigation, Methodology, Conceptualization, Writing—original draft; C.D.: Data curation, Visualization, Formal analysis, Writing—original draft; Y.C.: Supervision, Methodology, Funding acquisition, Conceptualization, Writing—review and editing; Y.K.: Methodology, Visualization; X.L.: Methodology, Writing—review and editing, Funding acquisition. All authors have read and agreed to the published version of the manuscript.

Funding: This work was supported by the National Engineering Research Center for Aluminum Smelting Technology Open Innovation Fund (No. ZYY2025KF02) and the Advanced Materials-National Science and Technology Major Project (No. 2025ZD0612200). The APC was funded by the National Engineering Research Center for Aluminum Smelting Technology Open Innovation Fund, grant number ZYY2025KF02.

Informed Consent Statement: Not applicable.

Data Availability Statement: The raw data supporting the conclusions of this article will be made available by the authors on request.

Conflicts of Interest: The authors declare no conflict of interest.

References

1. Gupta, A.; Basu, B. Sustainable Primary Aluminium Production: Technology Status and Future Opportunities. *Trans. Indian Inst. Met.* **2019**, *72*, 2135–2150. [CrossRef]
2. Chen, R.; Chen, Y.; Liang, X.; Kong, Y.; Fan, Y.; Liu, Q.; Yang, Z.; Tang, F.; Chabu, J.M.; Walle, M.D.; et al. Oxidative Exfoliation of Spent Cathode Carbon: A Two-in-One Strategy for Its Decontamination and High-Valued Application. *Chin. J. Chem. Eng.* **2023**, *59*, 262–269. [CrossRef]
3. Trowell, K.A.; Goroshin, S.; Frost, D.L.; Bergthorson, J. Aluminum and Its Role as a Recyclable, Sustainable Carrier of Renewable Energy. *Appl. Energy* **2020**, *275*, 115112. [CrossRef]
4. Haraldsson, J.; Johnsson, S.; Thollander, P.; Wallén, M. Taxonomy, Saving Potentials and Key Performance Indicators for Energy End-Use and Greenhouse Gas Emissions in the Aluminium Industry and Aluminium Casting Foundries. *Energies* **2021**, *14*, 3571. [CrossRef]
5. Ogoreltceva, N.; Fedorova, E.; Puzanov, I.; Zavadyak, A.; Nagibin, G.; Kirillova, I. Method of Protection of Cathode Blocks of Aluminium Electrolysis Cells. *Procedia Struct. Integr.* **2020**, *28*, 1340–1346. [CrossRef]
6. Cao, X.; Li, J.; Zhang, H.; Hu, H.; Zhao, Z.; Zhang, Q.; Liu, W.; Ren, M. Study on the Interface Deformation and Anode Current Distribution Variation in the Process of Anode Change in Aluminum Reduction Cell. In *Light Metals 2025*; Edwards, L., Ed.; Springer: Cham, Switzerland, 2025; pp. 484–496. [CrossRef]
7. Ilyushin, Y.V.; Kapostey, E.I. Developing a Comprehensive Mathematical Model for Aluminium Production in a Soderberg Electrolyser. *Energies* **2023**, *16*, 6313. [CrossRef]
8. Zhao, Z.; Gao, B.; Feng, Y.; Huang, Y.; Wang, Z.; Shi, Z.; Hu, X. Effects of Anode Wettability and Slots on Anodic Bubble Behavior Using Transparent Aluminium Electrolytic Cells. *JOM* **2017**, *69*, 281–291. [CrossRef]
9. Li, M.; Ma, S.; Li, H.; Hou, W.; Cheng, B.; Hu, T.; Wang, Y. Mode Coupling Analysis of Interfacial Stability and Critical Anode–Cathode Distance in a 500-kA Aluminum Electrolysis Cell. *JOM* **2021**, *73*, 2741–2751. [CrossRef]
10. Mohammad, I.; Dupuis, M.; Funkenbusch, P.D.; Kelley, D.H. Oscillating Currents Stabilize Aluminum Cells for Efficient, Low Carbon Production. *JOM* **2022**, *74*, 1908–1915. [CrossRef]
11. Zhou, S.; Diop, M.A.; Wang, Z.; Hu, X. Numerical Simulations of Copper Rod Insertion Effects on Current Density, Flow Field Distribution, Cathode Wear, and Electrothermal Dynamics in Aluminum Reduction Cells. In *Light Metals 2025*; Edwards, L., Ed.; Springer: Cham, Switzerland, 2025; pp. 518–526. [CrossRef]

12. Blais, M.; Désilets, M.; Lacroix, M. Optimization of the Cathode Block Shape of an Aluminum Electrolysis Cell. *Appl. Therm. Eng.* **2013**, *58*, 439–446. [CrossRef]
13. Liu, W.; Zhou, D.; Zhao, Z. Progress in Application of Energy-Saving Measures in Aluminum Reduction Cells. *JOM* **2019**, *71*, 2420–2429. [CrossRef]
14. Becasse, S.; Martin, O.; Allano, B.; Caratini, Y.; Tinka, D. APXe Cell Technology: 7 Years of Low Energy Operation. In *Light Metals 2018*; Martin, O., Ed.; Springer International Publishing: Cham, Switzerland, 2018; pp. 699–704. [CrossRef]
15. Zhou, S.; Diop, M.A.; Gao, B.; Wang, Z.; Hu, X.; Yang, Y.; Tao, W. Enhancing Sustainability in Aluminum Reduction Cells Through Cathode Repair Optimization and Numerical Simulations Study on Current Distribution and Erosion Hole Impact. *J. Sustain. Metall.* **2024**, *10*, 658–673. [CrossRef]
16. Hankel, J.; Kernebeck, S.; Deuerler, F.; Weber, S. Investigation of Phase Transformation Related Electrical Conductivity of Long-Term Heat Treated Aluminium Electrolysis Cathodes. *SN Appl. Sci.* **2022**, *4*, 215. [CrossRef]
17. Bojarevics, V. Effect of Cathode Collector Copper Inserts on the Hall-Héroult Cell MHD Stability. In *Light Metals 2016*; Williams, E., Ed.; Wiley: Hoboken, NJ, USA, 2016; pp. 933–938. [CrossRef]
18. Han, J.; Feng, B.; Chen, Z.; Liang, Z.; Chen, Y.; Liang, X. Simulation and Application of a New Type of Energy-Saving Steel Claw for Aluminum Electrolysis Cells. *Sustainability* **2024**, *16*, 8061. [CrossRef]
19. Feng, Y. Optimization of Horizontal Current in Metal Pad by Using Slotted Cathode and Heightened Collector Bars. In *Proceedings of the ICMMSE 2016*; Atlantis Press: Paris, France, 2016; pp. 188–193. [CrossRef]
20. Mahran, G.M.A.; Ali, M.M. Numerical Simulation of Cathodic Voltage Drop in Hall-Héroult Cell. *Miner. Eng.* **2020**, *157*, 106534. [CrossRef]
21. Song, Y.; Peng, J.; Di, Y.; Wang, Y.; Li, B.; Feng, N. The Impact of Cathode Material and Shape on Current Density in an Aluminum Electrolysis Cell. *JOM* **2016**, *68*, 593–599. [CrossRef]
22. Shi, Z.; Chai, D.; Huang, H.; Zhang, Y.; Fang, B. Technology Research on Decreasing the Aluminum Surface Waves and Reducing the Cathode Voltage Drop in Aluminum Electrolysis Cell. In *Light Metals 2016*, 1st ed.; Williams, E., Ed.; Wiley: Hoboken, NJ, USA, 2016; pp. 613–616. [CrossRef]
23. Gupta, A.; Jha, A.; Sahoo, M.; Jinil, J.; Nayak, J.P. Impact of Copper Insert on Low Amperage Aluminium Reduction Cell. In Proceedings of the 33rd International ICSOBA Conference, Dubai, United Arab Emirates, 29 November–1 December 2015; Travaux No. 44, Paper AL22. pp. 709–716.
24. Pfeffer, M.; Vera Garcia, O.; Hiltmann, F.; Bugnion, L. A Novel Cathode Design Using Copper Collector Bars for High Amperage Technologies. In Proceedings of the 39th International ICSOBA Conference, Manama, Bahrain, 22–24 November 2021; Travaux No. 50, Paper AL17; pp. 793–801.
25. Von Kaenel, R.; Antille, J.; Bugnion, L. Impact of Copper Inserts in Collector Bars. In *Light Metals 2015*; Hyland, M., Ed.; Springer International Publishing: Cham, Switzerland, 2015; pp. 807–812. [CrossRef]
26. Bastaki, M.; Zarouni, A.; Jonqua, B.; Ahli, N.; Mishra, L.; Al Jasmi, A.; Al Zarouni, A.; Reverdy, M.; Potocnik, V. Dubal Cell Voltage Drop Initiatives Towards Low Energy High Amperage Cells. In *Light Metals 2014*; Grandfield, J., Ed.; Springer International Publishing: Cham, Switzerland, 2014; pp. 451–455. [CrossRef]
27. Gupta, A.; Namboothiri, S. Impact of Carbon Seam on Freeze Profile in Aluminum Reduction Cell. *Trans. Indian Inst. Met.* **2017**, *70*, 1563–1574. [CrossRef]
28. Lalancette, F.; Désilets, M.; Pansiot, B.; LeBreux, M.; Bilodeau, J.-F. Dimensional Reduction of a 3D Thermoelectric Model to Create a Reliable and Time-Efficient 2D Model Representing an Aluminum Electrolysis Cell. *Int. J. Heat Mass Transf.* **2023**, *202*, 123777. [CrossRef]
29. Allard, F.; Désilets, M.; LeBreux, M.; Blais, A. Improved Heat Transfer Modeling of the Top of Aluminum Electrolysis Cells. *Int. J. Heat Mass Transf.* **2019**, *132*, 1262–1276. [CrossRef]
30. Dupuis, M. Computation of Aluminum Reduction Cell Energy Balance Using ANSYS® Finite Element Models. In *Essential Readings in Light Metals*; Bearne, G., Dupuis, M., Tarcy, G., Eds.; Springer: Cham, Switzerland, 2016; pp. 294–302. [CrossRef]
31. Ran, L.; Li, J.; Zou, Z.; Zhang, B.; Li, Q.; Yang, S.; Zhang, H. Interaction Investigation Between Ledge Evolution and Magnetohydrodynamic Flow Under Normal and Enhanced Current Conditions in Aluminum Reduction Cell. *Metall. Mater. Trans. B* **2025**, *56*, 2748–2767. [CrossRef]

Disclaimer/Publisher's Note: The statements, opinions and data contained in all publications are solely those of the individual author(s) and contributor(s) and not of MDPI and/or the editor(s). MDPI and/or the editor(s) disclaim responsibility for any injury to people or property resulting from any ideas, methods, instructions or products referred to in the content.